THE JOURNAL OF PHYSICAL CHEMISTRY A
A JOURNAL OF THE AMERICAN CHEMICAL SOCIETY

pubs.acs.org/JPCA

Article

Unconventional Stereoerror Formation Mechanisms in Nonmetallocene Propene Polymerization Systems Revealed by DFT Calculations

Published as part of The Journal of Physical Chemistry virtual special issue "Vincenzo Barone Festschrift".

Eugenio Romano, Peter H.M. Budzelaar, Claudio De Rosa, and Giovanni Talarico*

Cite This: *J. Phys. Chem. A* 2022, 126, 6203–6209

Read Online

ACCESS | Metrics & More | Article Recommendations | Supporting Information

ABSTRACT: An unconventional mechanism for the stereoerror formation in propene polymerization catalyzed by C_1-symmetric salalen-M systems (M = Zr, Hf) is suggested by DFT calculations. While propagation happens with the ligand in its *fac-mer* conformation, a change of ligand wrapping mode from *fac-mer* to *fac-fac* is the main source of the lower stereoselectivities obtained with Zr and Hf. This is different for the Ti analogues, where the ligand *fac-mer* wrapping mode does not play a role. Activation strain analysis indicates that the preference for a chain stationary mechanism of the Zr/Hf species is due to the energy required to distort the reactants (ΔE_{Strain}) rather than to their mutual interaction (ΔE_{Int}).

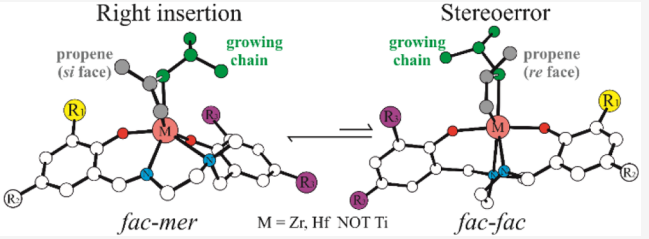

INTRODUCTION

The study of metallocene olefin polymerization catalysts has provided a detailed understanding of polymerization mechanisms, including stereoselectivity, regioselectivity, and molar mass capability.[1,2] Translation of these insights to new classes of catalysts has seemed straightforward, and this has in turn led to the vigorous development of new postmetallocene catalysts.[3−6] It is often implicitly assumed that the geometry of the active site corresponds to that of the neutral catalyst precursor, although exceptions are known.[7−13] In the case of C_1-symmetric catalysts, there are two diastereotopic active sites: propagation can happen predominantly without chain backskip ("Chain Migration mechanism", CM), predominantly with backskip after insertion ("Chain Stationary mechanism", CS), or any intermediate situation. For metallocenes, steric factors have been used to tune this balance (see Scheme 1A).[14−16] Interestingly, Kol et al.[17] reported on tuning of C_1-symmetric salalen complexes of Group 4, where it was proposed that the electronic asymmetry (due to the *trans* influence) was effective in enforcing a CS mechanism (see Scheme 1B). The ligand coordination mode of the active species was assumed to correspond to the *fac-mer* (FM) arrangement determined for the neutral catalyst precursor in the solid state.[17,18]

The FM coordination ensures the electronic asymmetry of the two coordination sites involved in polymerization because one coordination site is in *trans* to a phenoxy group and the other one *trans* to the sp^2 N atom (N_{imine}), see Figure 1A. However, DFT calculations indicate that the picture is more complicated: at least for Ti, the preferred wrapping mode for the cationic active species in propene polymerization is *fac-fac* (FF) (see Figure 1B), and the preferred FM conformation is slightly different from the one reported in the X-ray structure (see Figure 1C).[19]

The *trans* electronic influence is supposed to be less effective with the FF conformations, being dictated in that case by the different sp^2/sp^3 hybridization of the N atoms (N_{imine}/N_{amine}, respectively, Figure 1B), so limiting the directional site control of the chain. Understanding of the wrapping mode and hence the geometry of the active species is important not only for identifying the polymerization mechanism (e.g., chain stationary vs. chain migration) but also for successful ligand modification to enhance the stereoselectivity of the reaction. In particular, scattered and not yet explained results have been reported for the isoselectivity of propene polymerization (here considered as %[*mmmm*] detected by ^{13}C NMR spectra of the polypropylenes) promoted by salalen systems combined with Group 4 metals (M = Ti, Zr, Hf) and R_1, R_2, and R_3 ligand substituents (see Scheme 2).[18] We were particularly surprised by the (large) metal effect (with Ti much more stereoselective than the Zr and Hf analogues) and by the (minimal) ligand

Received: July 13, 2022
Revised: August 21, 2022
Published: September 2, 2022

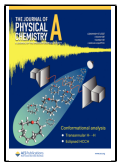

https://doi.org/10.1021/acs.jpca.2c04935
J. Phys. Chem. A 2022, 126, 6203−6209

Scheme 1. Steric and Electronic Effects for the Site Epimerization Mechanisms Proposed for C_1-Symmetric Active Species Based on *ansa*-Metallocenes (A) and Salalenes (B)[17]

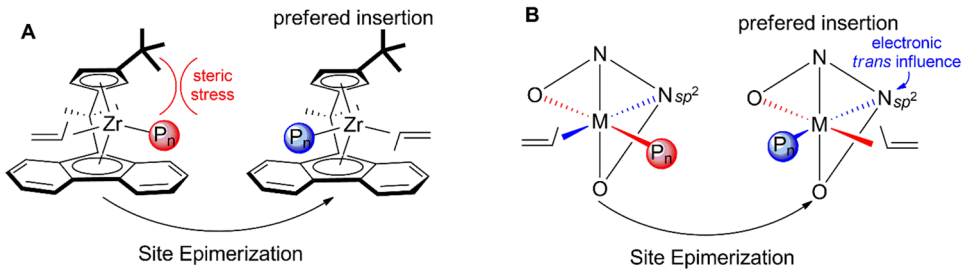

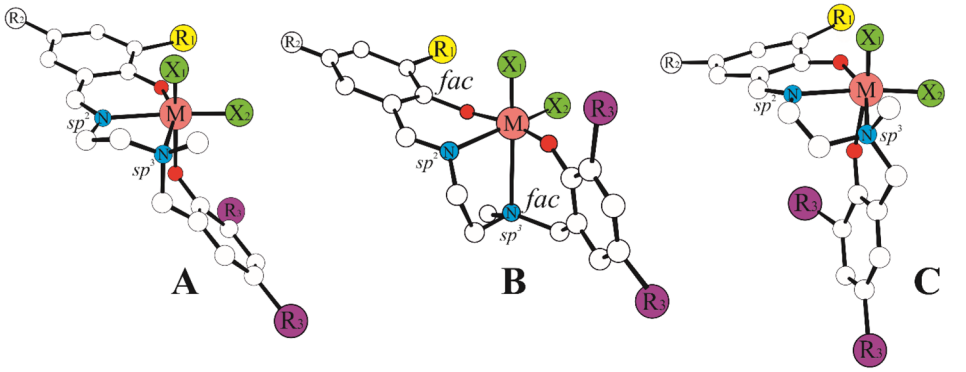

Figure 1. Coordination modes for salalen catalyst precursors with *fac-mer* (A), *fac-fac* (B), and a modified *fac-mer* ligand wrapping mode (C) reported for Ti systems.[19]

Scheme 2. Salalen Ligands Studied in This Work (Left) and Experimental Isoselectivity for Propene Polymerization Reported as %[*mmmm*] (Right)[18]

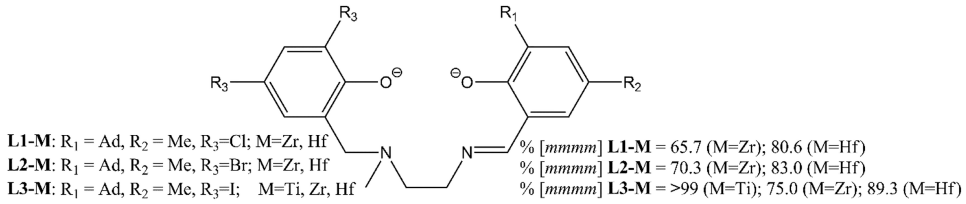

Table 1. Electronic Energy (Gibbs Free Energy) at DFT level (kcal/mol) for Propene Insertion TSs for Complexes with FM and FF Ligand Coordination Modes

ligand−metal	FF/FM[a]	$FF_{1/2}$[b]	$FM_{1/2}$[b]	FF_{Stereo}[c]	FM_{Stereo}[d]	$Calc_{Stereo}$[e]
L3-Ti	5.4 (5.3)	0.7 (0.6)	1.0 (1.6)	4.4 (4.4)	2.1 (2.3)	4.4 (4.4)
L1-Zr	−2.8 (−2.0)	0.8 (2.0)	5.9 (4.2)	3.0 (3.1)	3.6 (4.5)	2.8 (2.0)
L2-Zr	−2.3 (−1.9)	1.0 (1.8)	5.0 (4.2)	3.3 (2.7)	3.4 (4.0)	2.3 (1.9)
L3-Zr	−2.2 (−2.0)	1.0 (1.2)	4.8 (4.1)	3.8 (4.0)	3.4 (4.0)	2.2 (2.0)
L1-Hf	−2.8 (−1.6)	0.6 (1.0)	4.5 (3.8)	3.2 (3.7)	3.0 (2.6)	2.8 (1.6)
L2-Hf	−3.0 (−2.7)	1.5 (1.7)	5.6 (5.1)	3.0 (3.4)	3.4 (3.6)	3.0 (2.7)
L3-Hf	−2.6 (−2.7)	0.7 (1.3)	4.1 (4.1)	3.5 (3.9)	3.2 (4.3)	2.6 (2.7)

[a]Energy differences (free energies) of low-lying propene TSs at FM and FF structures (negative values indicate a preference for FM insertion. [b]Energy differences (free energies) of low-lying propene TSs at site 1 and site 2 for FF and FM species (positive values indicate a preference for site 1). [c]Calculated stereoselectivity at site 1 for FF structures. For definition of site 1 and site 2, see text and Figure 1. [d]Calculated stereoselectivity at site 1 for FM structures. For definition of site 1 and site 2, see text and Figure 1. [e]Calculated overall stereoselectivity including the contributions of all relevant ligand wrapping modes.

effect of increasing the bulkiness of R_3 substituents (going from Cl, Br to I) for Zr and Hf systems.

The latter aspect is remarkable because the R_3 "stereo-directing role" has been proposed as the main factor for explaining the stereoselectivity of octahedral complexes (both in homogeneous and heterogeneous phases)[20−23] (Figure S1). So, we decided to investigate in more detail the propene polymerization mechanisms of the Zr/Hf salalen catalysts shown in Scheme 2, using DFT calculations (see Computational Methods) combined with the Activation Strain Model (ASM).[24,25] The DFT computational approach has been already tested in propene polymerization catalysis and found to

https://doi.org/10.1021/acs.jpca.2c04935
J. Phys. Chem. A 2022, 126, 6203−6209

be reliable,[26,27] and in the ASM model,[24,25] the relative energy of a molecular system is partitioned into the sum of the energies required to distort the reactants into the geometries required to react and into the strength of their mutual interaction.[28,29]

COMPUTATIONAL METHODS

All DFT static calculations have been performed with the Gaussian09 and Gaussian16 set of programs,[30] using the B3LYP functional of Becke and Perdew.[31,32] The electronic configuration of the molecular systems was described with the standard split-valence basis set with a polarization function of Ahlrichs and co-workers for H, C, N, O, and Cl (SVP).[33] Stationary points were characterized using vibrational analyses, and these analyses were also used to calculate zero-point energies and thermal (enthalpy and entropy) corrections (298.15 K, 1 bar). Improved electronic energies were obtained from single-point calculations using a TZVP basis set[34] (SDD basis and pseudopotential[35] at the metal and Br, I), and the SVP-level enthalpy and entropy corrections, solvation (CPCM model,[36] toluene) and dispersion corrections[37] (EmpiricalDispersion = D3 in the Gaussian package). The growing polymer chains were simulated by ^{i}Bu groups and only the most stable TSs were reported for the insertion reactions. The variability of the results was also checked by using a different functional (ωB97XD)[38] showing differences below 1 kcal/mol. For the FM species, we found two conformations mode reported in Figure 1A/C; this implies that all transition state (TS) structures reported in the paper are calculated with both conformations and the lower energies (free energies) are reported in Table 1. The ASM-Energy Decomposition Analysis (EDA) model proposed by Bickelhaupt,[24,25] allows us to decompose the reaction energy profile into two contributions along the reaction coordinate: $\Delta E = \Delta E_{Strain} + \Delta E_{Int}$ where ΔE_{Strain} is the energy related to reactant deformation into the geometries required to react and ΔE_{Int} is the energy related to the strength of their mutual interactions. The former term is the sum of the strain related with each reactant: $\Delta E_{Strain} = \Delta E_{Strain,frag1} + \Delta E_{Strain,frag2}$ where $\Delta E_{Strain,frag1}$ and $\Delta E_{Strain,frag2}$ are the deformation energies of the fragment 1 and fragment 2 corresponding in our case to active specie plus growing polymer chain ($\Delta E_{Strain(Cat)}$) and the propene molecule ($\Delta E_{Strain(C3H6)}$), calculated with respect to minimum equilibrium geometry of the fragments. The latter term has been decomposed using the NEDA (Natural Energy Decomposition Analysis) scheme.[39] We applied this analysis to each point obtained by IRC calculations, and $\Delta E_{Strain(Cat)}$ and $\Delta E_{Strain(C3H6)}$ have been obtained from the ASM by subtracting the energy of the minimum equilibrium geometry from the energy of the respective fragment. Simultaneously, the NEDA scheme on each point of the scan (using NBO version 7 on Gaussian16) using a TZVP basis set[34] (SDD basis and pseudopotential at the metal)[35] and considering only dispersion corrections[37] has been performed, obtaining ΔE_{Int} and all its components (electrostatic, polarization, charge transfer, exchange, and deformation components).

RESULTS AND DISCUSSION

Let us start the discussion by analyzing the DFT results for the propene insertion TS at the systems of Scheme 2 with M = Ti, Zr, Hf reported in Table 1. The variability of the preferred coordination mode and the existence of diastereotopic reactive

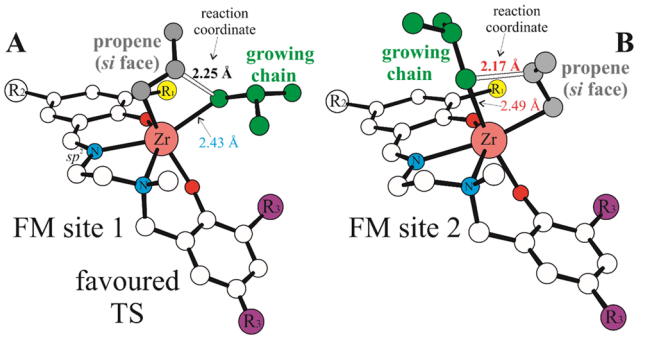

Figure 2. DFT optimized geometries for propene insertion (*si* face) TSs promoted by **L1-Zr** with FM ligand coordination mode: site 1 (A) and site 2 (B). H atoms omitted for clarity, distances in Å.

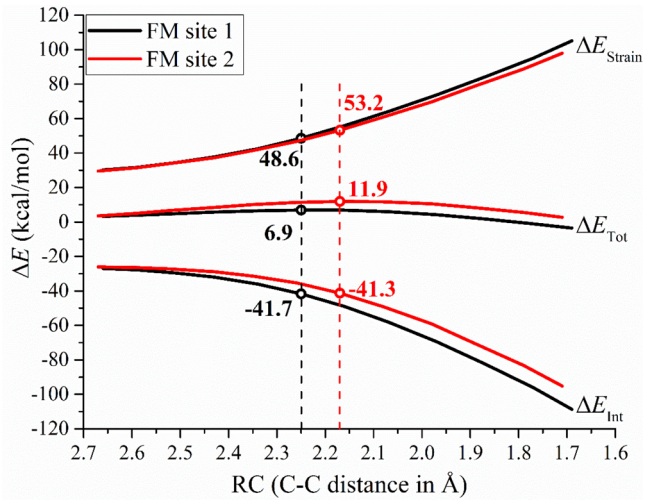

Figure 3. ASM analysis of the propene insertion at site 1 (black) and site 2 (red) of system **L1-Zr** in FM coordination mode as a function of the reaction coordinate. With circles are reported the values (kcal/mol) calculated at the two TS structures.

sites shown in Figure 1 necessitated the calculation of 18 TSs per ligand. We label as "site 1" the olefin insertion in the position of X_1 and the chain in the position of X_2 (see Figure 1) for both FF and FM structures. This computational screening is summarized in Table 1, and we use the following definition for the sake of readability: (a) FF/FM (second column) is the energy difference (Gibbs free energy difference) between the lower-lying propene insertion TSs at FM and FF coordination modes, (positive values indicate a preference for FF); (b) $FF_{1/2}$ and $FM_{1/2}$ (third and fourth columns) report energy differences of propene TSs at sites 1 and 2 for FF and FM species, respectively, (positive values indicate a preference for site 1); (c) FF_{Stereo} and FM_{Stereo} values (fifth and sixth column) are the stereoselectivities calculated at the active species with FF and FM coordination modes; (d) $Calc_{Stereo}$ (final column) is our computational estimate for the propene enantioface selection including the contributions of all relevant ligand wrapping modes.

The first interesting result is that for Zr and Hf systems the preferred propene insertion occurs at FM geometry for **L1-L3** ligands. This is the opposite of what we found earlier for Ti complexes[19] (see FF/FM results in Table 1) but is consistent with Kol's proposal for Zr and Hf.[18] Considering the $FM_{1/2}$ values, the energy difference between the propene insertion at

https://doi.org/10.1021/acs.jpca.2c04935
J. Phys. Chem. A 2022, 126, 6203−6209

Table 2. ASM Analysis for the Propene Reaction Coordinate (RC, in Å) at the Two Diastereotopic Active Sites (Site 1 on the Left and Site 2 on the Right) of L1-Zr Complex[a]

RC (Å)	ΔE_{Strain} site 1	ΔE_{Int} site 1	ΔE_{Tot} site 1	ΔE_{Strain} (Cat) site 1	ΔE_{Strain} (C3H6) site 1	RC (Å)	ΔE_{Strain} site 2	ΔE_{Int} site 2	ΔE_{Tot} site 2	ΔE_{Strain} (Cat) site 2	ΔE_{Strain} (C3H6) site 2
1.69	105.1	-108.7	-3.5	42.7	62.4	1.71	97.9	-95.2	2.7	43.0	54.9
1.77	95.0	-96.1	-1.0	40.1	54.9	1.79	88.8	-83.2	5.6	40.4	48.4
1.87	84.1	-82.4	1.8	37.4	46.7	1.89	78.9	-70.6	8.3	38.1	40.8
1.97	73.7	-69.4	4.3	35.2	38.5	1.98	69.7	-59.1	10.6	36.2	33.5
2.07	64.1	-58.0	6.0	33.1	30.9	2.08	60.9	-49.2	11.8	34.3	26.6
2.16	55.9	-49.0	6.9	31.5	24.4	**2.17**	**53.2**	**-41.3**	**11.9**	**32.6**	**20.6**
2.25	**48.6**	**-41.7**	**6.9**	**29.9**	**18.8**	2.26	46.7	-35.3	11.3	31.3	15.4
2.34	42.5	-36.0	6.5	28.6	13.9	2.35	41.5	-31.4	10.1	30.0	11.5
2.43	37.7	-32.0	5.8	27.5	10.3	2.43	37.3	-28.8	8.5	28.8	8.5
2.51	34.4	-29.6	4.8	26.6	7.8	2.52	34.0	-27.3	6.7	27.7	6.3
2.59	31.7	-27.7	4.0	25.8	5.9	2.59	31.5	-26.5	5.0	26.7	4.7
2.66	30.2	-26.9	3.3	25.3	5.0	2.67	29.6	-26.1	3.5	25.9	3.7

[a]In bold are reported the values obtained at the TS geometries (black for site 1 and red for site 2, respectively). Values in kcal/mol.

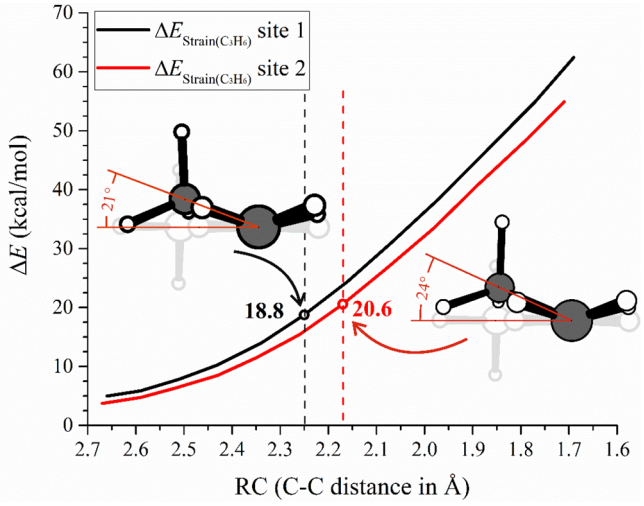

Figure 4. ASM analysis of the $\Delta E_{Strain(C3H6)}$ for propene insertion at site 1 (black) and site 2 (red) of **L1-Zr** as a function of the reaction coordinate. With circles are reported the values (kcal/mol) calculated at the TS structures. The olefin deformation is reported with respect to the free olefin (light gray).

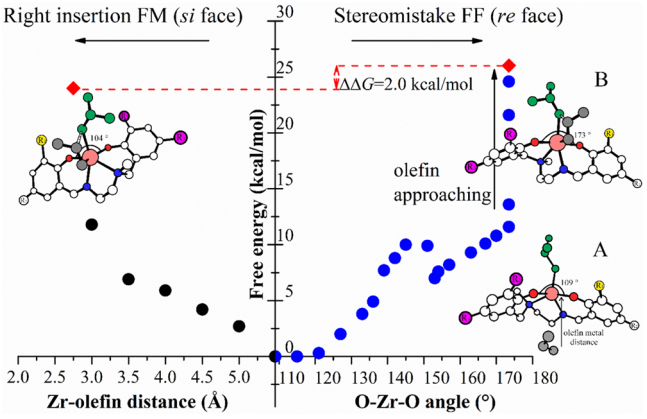

Figure 6. DFT calculated path of ligand O−Zr−O angle variation (from A) and further olefin capture (B) leading from penta-coordinated **LZr(P)**$^+$ to hexacoordinate FF olefin insertions (left) and the analogous path for the FM insertion (right) where the initial O−Zr−O is already close to the one calculated at the TS geometry.

the two reaction sites (4−6 kcal/mol, see Table 1) is remarkable and similar for all three metals: this leads to an expected CS mechanism at site 1 for Zr and Hf (but not for Ti because it does not propagate through FM). The TS geometries of the preferred propene insertion at the two diastereotopic sites for **L1-Zr** system are shown in Figure 2; both sites prefer the same propene enantioface, and as expected, insertion at the site 1 having the growing chain

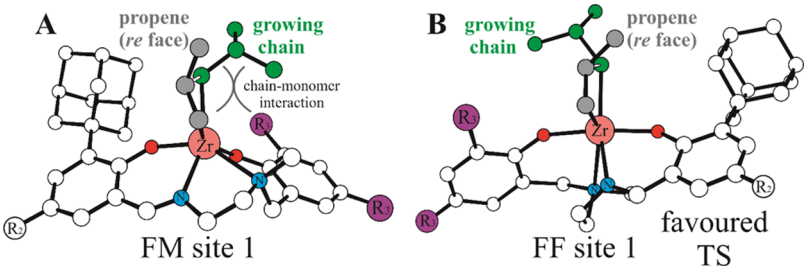

Figure 5. DFT optimized geometries for propene stereoerror insertion (*re* face) TSs promoted by **L1-Zr** with FM (A) and FF (B) coordination modes at site 1. H atoms omitted for clarity, R_2 = Me; R_3 = Cl.

https://doi.org/10.1021/acs.jpca.2c04935
J. Phys. Chem. A 2022, 126, 6203−6209

Scheme 3. General Scheme Achieved by DFT Calculations Summarizing the Catalyst Precursor Structure, the Ligand Wrapping Mode of the Active Species, the Calculated Stereoselectivity, and the Substituent Effects on Propene Polymerization Promoted by Salalen-Ligand with M = Ti, Zr, Hf

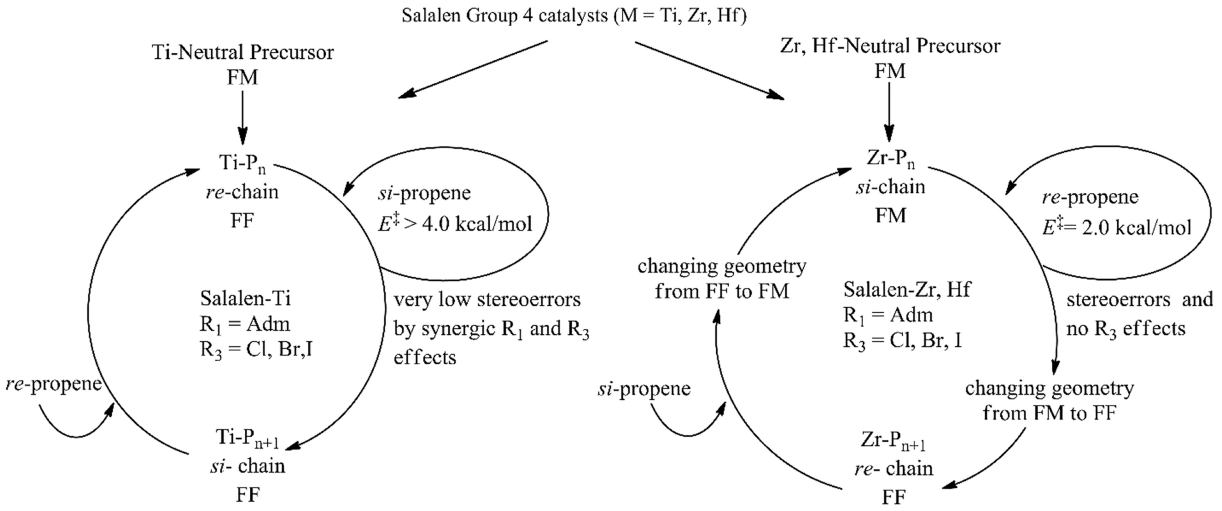

trans to the N_{imine}, (Figure 2A) is favored with respect to site 2 (Figure 2B).

Overall, these results seem to give additional credit to the idea of Kol et al. concerning the use of electronic effects—dictated by the FM wrapping mode—to control the chain direction (Scheme 1B).[17] Coherently, this effect is reduced to ∼1 kcal/mol for the FF geometries (see $FF_{1/2}$ values, third column). Considering the possibility that a combination of steric *plus* electronic influence might enhance our control of polymerization, we decided to further explore this aspect using the ASM approach.[24,25] In the insertion reaction considered here, the two fragments are the catalyst carrying the growing polymer chain and the propene molecule as described in the Computational Methods section. The Figure 3 reports the activation strain diagram of propene insertion promoted by **L1-Zr** system with the total energy (ΔE_{Tot}) and its decomposition terms, the total strain energy (ΔE_{Strain}) and total interaction energy (ΔE_{Int}) against the reaction coordinate (RC) assumed as the $C_{C3H6}-C_{chain}$ distance of the forming bond (see Figure 2), with the positions of the corresponding TSs indicated by circles.

Surprisingly, we find that the main contribution to the ΔE_{Tot} energetic difference (5 kcal/mol, see Figure 3) is due to ΔE_{Strain} and not to ΔE_{Int} as might be expected if considering the electronic *trans* influence (Scheme 1B). This may be due, in part, to the fact that the insertion TS at site 2 occurs at a smaller distance (2.17 Å) than at site 1 (2.25 Å); thus, the olefin needs to come in closer contact with the chain, implying more deformation of both olefin and catalyst. In any case, the two terms composing ΔE_{Strain} ($\Delta E_{Strain(Cat)}$ and $\Delta E_{Strain(C3H6)}$) both point to a lower deformation energy of the catalyst carrying the chain and olefin at site 1 (see Table 2).

Focusing on the olefin deformation, Figure 4 shows the $\Delta E_{Strain(C3H6)}$ trend for site 1 and site 2. Although the graph indicates greater olefin deformation at site 1 for equal C−C distances, by looking at the TS geometries we find that olefin deformation at site 1 costs less energy than at site 2. In Figure 4, the deformed olefin is compared to the planar free olefin with the angle in red representing the hypothetical dihedral angle H−C−C−CH_3 that would form with the H atom in the horizontal plane. It is evident that the olefin at both TSs needs to be deformed to insert in the metal−carbon bond, but the methyl group deformation is less pronounced at site 1 than site 2.

While the difference in propagating species (Ti: FF; Zr/Hf: FM) is interesting, this does not by itself explain the lower stereoselectivity of the Zr/Hf systems.[17,18] One could imagine that FM is intrinsically less stereoselective than FF,[40,41] but our computational results do not support this. In fact, the FM_{Stereo} results in Table 1 show that stereoselectivity of FM insertion is even higher for Zr/Hf (>3 kcal/mol) than for Ti (2.4 kcal/mol).

The lowest TS we found for a propene stereomistake at the FM geometry is shown in Figure 5A (additional conformations with higher energies are reported in Figure S2). The bulky R_1 substituent (adamantyl for ligands **L1**−**L3**) forces the chain to adopt a conformation *syn* to the methyl group of the propene *re* face.[20,21] However, we find that for Zr/Hf the FF wrapping mode is accessible. Since FF insertion happens with the opposite enantioface, this turns out to be the main source of stereoerrors for Zr/Hf; Figure 5B shows the lowest FF insertion TS. In contrast, for Ti, the FM mode is not accessible and hence plays no role in stereoregulation.

In addition, the R_3 substituents are far away from monomer and growing chain in the FF geometries (Figure 5B), which may account for the ineffectiveness of substituent bulk to tune the calculated (see $Calc_{Stereo}$ column in Table 1) and experimental isoselectivity of Zr and Hf salalen complexes reported in Scheme 2.

To the best of our knowledge, variation of ligand wrapping mode inducing the formation of a stereoerror has not been reported in TM-catalyzed olefin polymerization. Fluxionality of active sites during the polymerization chain growth has been suggested for heterogeneous Ziegler−Natta systems[21,42,43] as well as oscillating metallocene catalysts[44] or bisphenoxyimine systems.[45] However, for the first two cases, the modification of active site geometries produces stereoblock microstructures[21] (and not an occasional stereomistake), whereas in the latter case, the interconversion between Δ and Λ forms is dictated at each insertion step.[46]

For our explanation to work, it is important that changes in ligand wrapping mode can happen easily. To test this point, we

https://doi.org/10.1021/acs.jpca.2c04935
J. Phys. Chem. A 2022, 126, 6203−6209

traced the path of interconversion from the pentacoordinated Zr species to the two TSs (Figure 6) on approach of the propene monomer. The pentacoordinated species (see structure A on Figure 6, right) shows the O−Zr−O angle of 109°, which is close to the one reported in the TS of the FM stereoregular insertion (Figure 6, left), whereas this angle has to increase to 173° for the FF insertion TS followed by the olefin approaching (see structure B on Figure 6, right). The results show that conformational change is possible without a significant intervening barrier, which can explain the nonblocky nature of stereoerror insertion for this system.

CONCLUSIONS

The above considerations are summarized in different catalytic cycles proposed for Ti and Zr/Hf salalen systems (Scheme 3).

The Ti active species features a ligand wrapping mode (FF) that differs from its neutral precursor (FM) but is otherwise "normal" in its mechanism of stereoerror formation. In contrast, the Zr and Hf active species propagate as FM but generate stereoerrors via easy formation of an FF-wrapped mode. The easy accessibility of the Zr FF wrapping mode explains the formation of isolated stereoerrors, differing sharply from cases of "oscillating" catalysts where active species interconversion is slow on the propagation time scale.[47,48] Thus, active species fluxionality (and/or change in the wrapping mode) is yet another factor to keep in mind when tuning the polypropylene microstructure analogously to the peculiar chiral recognition recently reported on the stereocontrolled ring-opening polymerization of lactide.[49−51]

ASSOCIATED CONTENT

Supporting Information

The Supporting Information is available free of charge at https://pubs.acs.org/doi/10.1021/acs.jpca.2c04935.

Figures S1 and S2 (PDF)

Cartesian coordinates of the structures discussed in the text (XYZ)

AUTHOR INFORMATION

Corresponding Author

Giovanni Talarico − *Scuola Superiore Meridionale, 80138 Napoli, Italy; Dipartimento di Scienze Chimiche, Università degli Studi di Napoli Federico II, 80126 Napoli, Italy;* orcid.org/0000-0002-4861-0444; Email: talarico@unina.it

Authors

Eugenio Romano − *Scuola Superiore Meridionale, 80138 Napoli, Italy;* orcid.org/0000-0001-7902-490X

Peter H.M. Budzelaar − *Dipartimento di Scienze Chimiche, Università degli Studi di Napoli Federico II, 80126 Napoli, Italy;* orcid.org/0000-0003-0039-4479

Claudio De Rosa − *Dipartimento di Scienze Chimiche, Università degli Studi di Napoli Federico II, 80126 Napoli, Italy;* orcid.org/0000-0002-5375-7475

Complete contact information is available at: https://pubs.acs.org/10.1021/acs.jpca.2c04935

Author Contributions

The manuscript was written through contributions of all authors. All authors have given approval to the final version of the manuscript.

Notes

The authors declare no competing financial interest.

ACKNOWLEDGMENTS

This work was supported by grant "Ricerca di Ateneo, DR_409_2017" of the Università di Napoli Federico II.

REFERENCES

(1) Resconi, L.; Cavallo, L.; Fait, A.; Piemontesi, F. Selectivity in Propene Polymerization with Metallocene Catalysts. *Chem. Rev.* **2000**, *100*, 1253−1346.

(2) Talarico, G.; Budzelaar, P. H. M. Variability of Chain Transfer to Monomer Step in Olefin Polymerization. *Organometallics* **2008**, *27*, 4098−4107.

(3) Gibson, V. C.; Spitzmesser, S. K. Advances in Non-Metallocene Olefin Polymerization Catalysis. *Chem. Rev.* **2003**, *103*, 283−315.

(4) Busico, V.; Cipullo, R.; Pellecchia, R.; Ronca, S.; Roviello, G.; Talarico, G. Design of stereoselective Ziegler-Natta propene polymerization catalysts. *Proc. Natl. Acad. Sci. U. S. A.* **2006**, *103*, 15321−15326.

(5) Boussie, T. R.; Diamond, G. M.; Goh, C.; Hall, K. A.; LaPointe, A. M.; Leclerc, M. K.; Murphy, V.; Shoemaker, J. A. W.; Turner, H.; Rosen, R. K.; Stevens, J. C.; Alfano, F.; Busico, V.; Cipullo, R.; Talarico, G. Nonconventional Catalysts for Isotactic Propene Polymerization in Solution Developed by Using High-Throughput-Screening Technologies. *Angew. Chem., Int. Ed.* **2006**, *45*, 3278−3283.

(6) Baier, M. C.; Zuideveld, M. A.; Mecking, S. Post-Metallocenes in the Industrial Production of Polyolefins. *Angew. Chem., Int. Ed.* **2014**, *53*, 9722−9744.

(7) Froese, R. D. J.; Hustad, P. D.; Kuhlman, R. L.; Wenzel, T. T. Mechanism of Activation of a Hafnium Pyridyl-Amide Olefin Polymerization Catalyst: Ligand Modification by Monomer. *J. Am. Chem. Soc.* **2007**, *129*, 7831−7840.

(8) Busico, V.; Cipullo, R.; Pellecchia, R.; Rongo, L.; Talarico, G.; Macchioni, A.; Zuccaccia, C.; Froese, R. D. J.; Hustad, P. D. Uni et Trini": In Situ Diversification of (Pyridylamide)hafnium(IV) Catalysts. *Macromolecules* **2009**, *42*, 4369−4373.

(9) Domski, G. J.; Edson, J. B.; Keresztes, I.; Lobkovsky, E. B.; Coates, G. W. Synthesis of a new olefin polymerization catalyst supported by an sp^3-C donor *via* insertion of a ligand-appended alkene into the Hf-C bond of a neutral pyridylamidohafnium trimethyl complex. *Chem. Commun.* **2008**, 6137−6139.

(10) Zuccaccia, C.; Busico, V.; Cipullo, R.; Talarico, G.; Froese, R. D. J.; Vosejpka, P. C.; Hustad, P. D.; Macchioni, A. On the First Insertion of a-Olefins in Hafnium Pyridyl-Amido Polymerization Catalysts. *Organometallics* **2009**, *28*, 5445−5458.

(11) De Rosa, C.; Di Girolamo, R.; Muñoz-García, A. B.; Pavone, M.; Talarico, G. Breaking Symmetry Rules Enhance the Options for Stereoselective Propene Polymerization Catalysis. *Macromolecules* **2020**, *53*, 2959−2964.

(12) Domski, G. J.; Eagan, J. M.; De Rosa, C.; Di Girolamo, R.; LaPointe, A. M.; Lobkovsky, E. B.; Talarico, G.; Coates, G. W. Combined Experimental and Theoretical Approach for Living and Isoselective Propylene Polymerization. *ACS Catal.* **2017**, *7*, 6930−6937.

(13) De Rosa, C.; Di Girolamo, R.; Talarico, G. Expanding the Origin of Stereocontrol in Propene Polymerization Catalysis. *ACS Catal.* **2016**, *6*, 3767−3770.

(14) Miller, S. A.; Bercaw, J. E. Mechanism of Isotactic Polypropylene Formation with C_1-Symmetric Metallocene Catalysts. *Organometallics* **2006**, *25*, 3576−3592.

(15) Castro, L.; Therukauff, G.; Vantomme, A.; Welle, A.; Haspeslagh, L.; Brusson, J.-M.; Maron, L.; Carpentier, J.-F.; Kirillov, E. A Theoretical Outlook on the Stereoselectivity Origins of Isoselective Zirconocene Propylene Polymerization Catalysts. *Chem.—Eur. J.* **2018**, *24*, 10784−10792.

(16) Motta, A.; Fragalà, I. L.; Marks, T. J. Stereochemical Control Mechanisms in Propylene Polymerization Mediated by C_1-Symmetric

CGC Titanium Catalyst Centers. *J. Am. Chem. Soc.* **2007**, *129*, 7327−7338.
(17) Press, K.; Cohen, A.; Goldberg, I.; Venditto, V.; Mazzeo, M.; Kol, M. Salalen Titanium Complexes in the Highly Isospecific Polymerization of 1-Hexene and Propylene. *Angew. Chem., Int. Ed.* **2011**, *50*, 3529−3532.
(18) Press, K.; Venditto, V.; Goldberg, I.; Kol, M. Zirconium and hafnium Salalen complexes in isospecific polymerisation of propylene. *Dalton Trans.* **2013**, *42*, 9096−9103.
(19) Talarico, G.; Budzelaar, P. H. M. Ligand Coordination Driven by Monomer and Polymer Chain: The Intriguing Case of Salalen-Ti Catalyst for Propene Polymerization. *Macromolecules* **2017**, *50*, 5332−5336.
(20) Corradini, P.; Barone, V.; Fusco, R.; Guerra, G. A possible model of catalytic sites for the stereospecific polymerization of a-olefins on first-generation and supported Ziegler-Natta catalysts. *Gazz. Chim. Ital.* **1983**, *113*, 601−607.
(21) Bahri-Laleh, N.; Hanifpour, A.; Mirmohammadi, S. A.; Poater, A.; Nekoomanesh-Haghighi, M.; Talarico, G.; Cavallo, L. Computational modeling of heterogeneous Ziegler-Natta catalysts for olefins polymerization. *Prog. Polym. Sci.* **2018**, *84*, 89−114.
(22) Cipullo, R.; Busico, V.; Fraldi, N.; Pellecchia, R.; Talarico, G. Improving the Behavior of Bis(phenoxyamine) Group 4 Metal Catalysts for Controlled Alkene Polymerization. *Macromolecules* **2009**, *42*, 3869−3872.
(23) Corradini, P.; Guerra, G.; Cavallo, L. Do New Century Catalysts Unravel the Mechanism of Stereocontrol of Old Ziegler-Natta Catalysts? *Acc. Chem. Res.* **2004**, *37*, 231−241.
(24) Vermeeren, P.; van der Lubbe, S. C. C.; Fonseca Guerra, C.; Bickelhaupt, F. M.; Hamlin, T. A. Understanding chemical reactivity using the activation strain model. *Nat. Protoc.* **2020**, *15*, 649−667.
(25) Bickelhaupt, F. M.; Houk, K. N. Analyzing Reaction Rates with the Distortion/Interaction-Activation Strain Model. *Angew. Chem., Int. Ed.* **2017**, *56*, 10070−10086.
(26) Falivene, L.; Cavallo, L.; Talarico, G. Buried Volume Analysis for Propene Polymerization Catalysis Promoted by Group 4 Metals: A Tool for Molecular Mass Prediction. *ACS Catal.* **2015**, *5*, 6815−6822.
(27) Falivene, L.; Barone, V.; Talarico, G. Unraveling the role of entropy in tuning unimolecular *vs.* bimolecular reaction rates: The case of olefin polymerization catalyzed by transition metals. *Mol. Catal.* **2018**, *452*, 138−144.
(28) Zhao, Y.; Xu, X.; Wang, Y.; Liu, T.; Li, H.; Zhang, Y.; Wang, L.; Wang, X.; Zhao, S.; Luo, Y. Ancillary ligand effects on α-olefin polymerization catalyzed by zirconium metallocene: a computational study. *RSC Adv.* **2022**, *12*, 21111−21121.
(29) Núñez-Zarur, F.; Comas-Vives, A. Understanding the Olefin Polymerization Initiation Mechanism by Cr(III)/SiO_2 Using the Activation Strain Model. *J. Phys. Chem. C* **2022**, *126*, 296−308.
(30) Frisch, M. J.; Trucks, G. W.; Schlegel, H. B.; Scuseria, G. E.; Robb, M. A.; Cheeseman, J. R.; Scalmani, G.; Barone, V.; Petersson, G. A.; Nakatsuji, H.; et al. *Gaussian 16, Revision A.01*; Gaussian, Inc.: Wallingford, CT, 2016.
(31) Becke, A. Density-functional exchange-energy approximation with correct asymptotic behavior. *Phys. Rev. A* **1988**, *38*, 3098−3100.
(32) Perdew, J. P. Density-functional approximation for the correlation energy of the inhomogeneous electron gas. *Phys. Rev. B* **1986**, *33*, 8822−8824.
(33) Schäfer, A.; Horn, H.; Ahlrichs, R. Fully optimized contracted Gaussian basis sets for atoms lithium to krypton. *J. Chem. Phys.* **1992**, *97*, 2571−2577.
(34) Weigend, F.; Furche, F.; Ahlrichs, R. Gaussian basis sets of quadruple zeta valence quality for atoms H-Kr. *J. Chem. Phys.* **2003**, *119*, 12753−12762.
(35) Bergner, A.; Dolg, M.; Kuechle, W.; Stoll, H.; Preuss, H. Ab initio energy-adjusted pseudopotentials for elements of groups 13−17. *Mol. Phys.* **1993**, *80*, 1431−1441.
(36) Barone, V.; Cossi, M. Quantum Calculation of Molecular Energies and Energy Gradients in Solution by a Conductor Solvent Model. *J. Phys. Chem. A* **1998**, *102*, 1995−2001.
(37) Grimme, S.; Antony, J.; Ehrlich, S.; Krieg, H. A consistent and accurate ab initio parametrization of density functional dispersion correction (DFT-D) for the 94 elements H-Pu. *J. Chem. Phys.* **2010**, *132*, 154104.
(38) Chai, J.-D.; Head-Gordon, M. Long-range corrected hybrid density functionals with damped atom-atom dispersion corrections. *Phys. Chem. Chem. Phys.* **2008**, *10*, 6615−6620.
(39) Glendening, E. D. Natural Energy Decomposition Analysis: Explicit Evaluation of Electrostatic and Polarization Effects with Application to Aqueous Clusters of Alkali Metal Cations and Neutrals. *J. Am. Chem. Soc.* **1996**, *118*, 2473−2482.
(40) Talarico, G.; Budzelaar, P. H. M. Analysis of Stereochemistry Control in Homogeneous Olefin Polymerization Catalysis. *Organometallics* **2014**, *33*, 5974−5982.
(41) Talarico, G.; Budzelaar, P. H. M. α-Agostic Interactions and Growing Chain Orientation for Olefin Polymerization Catalysts. *Organometallics* **2016**, *35*, 47−54.
(42) De Rosa, C.; Ruiz de Ballesteros, O.; Di Girolamo, R.; Malafronte, A.; Auriemma, F.; Talarico, G.; Scoti, M. The blocky structure of Ziegler-Natta "random" copolymers: myths and experimental evidence. *Polym. Chem.* **2020**, *11*, 34−38.
(43) De Rosa, C.; Ruiz de Ballesteros, O.; Auriemma, F.; Talarico, G.; Scoti, M.; Di Girolamo, R.; Malafronte, A.; Piemontesi, F.; Liguori, D.; Camurati, I.; et al. Crystallization Behavior of Copolymers of Isotactic Poly(1-butene) with Ethylene from Ziegler-Natta Catalyst: Evidence of the Blocky Molecular Structure. *Macromolecules* **2019**, *52*, 9114−9127.
(44) Coates, G. W.; Waymouth, R. M. Oscillating Stereocontrol: A Strategy for the Synthesis of Thermoplastic Elastomeric Polypropylene. *Science* **1995**, *267*, 217−219.
(45) Makio, H.; Terao, H.; Iwashita, A.; Fujita, T. FI Catalysts for Olefin Polymerization-A Comprehensive Treatment. *Chem. Rev.* **2011**, *111*, 2363−2449.
(46) Milano, G.; Cavallo, L.; Guerra, G. Site Chirality as a Messenger in Chain-End Stereocontrolled Propene Polymerization. *J. Am. Chem. Soc.* **2002**, *124*, 13368−13369.
(47) Lin, S.; Tagge, C. D.; Waymouth, R. M.; Nele, M.; Collins, S.; Pinto, J. C. Kinetics of Propylene Polymerization Using Bis(2-phenylindenyl)zirconium Dichloride/Methylaluminoxane. *J. Am. Chem. Soc.* **2000**, *122*, 11275−11285.
(48) Busico, V.; Cipullo, R.; Kretschmer, W. P.; Talarico, G.; Vacatello, M.; Van Axel Castelli, V. Oscillating" Metallocene Catalysts: How Do They Oscillate? *Angew. Chem., Int. Ed.* **2002**, *41*, 505−508.
(49) D'Alterio, M. C.; De Rosa, C.; Talarico, G. Syndiotactic PLA from *meso*-LA polymerization at the Al-chiral complex: a probe of DFT mechanistic insights. *Chem. Commun.* **2021**, *57*, 1611−1614.
(50) D'Alterio, M. C.; De Rosa, C.; Talarico, G. Stereoselective Lactide Polymerization: the Challenge of Chiral Catalyst Recognition. *ACS Catal.* **2020**, *10*, 2221−2225.
(51) Han, J. W.; Hollmann, F.; Luque, R.; Song, I. K.; Talarico, G.; Tatsumi, T.; Yan, N. Molecular Catalysis for the Chemistry of the future: a perspective. *Mol. Catal.* **2022**, *522*, 112233.

https://doi.org/10.1021/acs.jpca.2c04935
J. Phys. Chem. A 2022, 126, 6203−6209